ChemPubSoc Europe

DOI: 10.1002/chem.201604835

CHEMISTRY A European Journal Full Paper

Quantum Tunneling |*Hot Paper*|

Quenching the Quantum Tunneling of Magnetization in Heterometallic Octanuclear {$TM^{III}_4Dy^{III}_4$} (TM = Co and Cr) Single-Molecule Magnets by Modification of the Bridging Ligands and Enhancing the Magnetic Exchange Coupling

Kuduva R. Vignesh,[b] Stuart K. Langley,[c] Keith S. Murray,*[d] and Gopalan Rajaraman*[a]

Abstract: We report the synthesis, structural characterisation, magnetic properties and provide an ab initio analysis of the magnetic behaviour of two new heterometallic octanuclear coordination complexes containing Co^{III} and Dy^{III} ions. Single-crystal X-ray diffraction studies revealed molecular formulae of $[Co^{III}_4Dy^{III}_4(\mu\text{-OH})_4(\mu_3\text{-OMe})_4\{O_2CC(CH_3)_3\}_4(tea)_4(H_2O)_4]\cdot 4H_2O$ (**1**) and $[Co^{III}_4Dy^{III}_4(\mu\text{-F})_4(\mu_3\text{-OH})_4(o\text{-tol})_8(mdea)_4]\cdot 3H_2O\cdot EtOH\cdot MeOH$ (**2**; tea^{3-} = triply deprotonated triethanolamine; $mdea^{2-}$ = doubly deprotonated *N*-methyldiethanolamine; *o*-tol = *o*-toluate), and both complexes display an identical metallic core topology. Furthermore, the theoretical, magnetic and SMM properties of the isostructural complex, $[Cr^{III}_4Dy^{III}_4(\mu\text{-F}_4)(\mu_3\text{-OMe})_{1.25}(\mu_3\text{-OH})_{2.75}(O_2CPh)_8(mdea)_4]$ (**3**), are discussed and compared with a structurally similar complex, $[Cr^{III}_4Dy^{III}_4(\mu_3\text{-OH})_4(\mu\text{-N}_3)_4(mdea)_4(O_2CC(CH_3)_3)_4]$ (**4**). DC and AC magnetic susceptibility data revealed single-molecule magnet (SMM) behaviour for **1**–**4**. Each complex displays dynamic behaviour, highlighting the effect of ligand and transition metal ion replacement on SMM properties. Complexes **2**, **3** and **4** exhibited slow magnetic relaxation with barrier heights (U_{eff}) of 39.0, 55.0 and 10.4 cm^{-1} respectively. Complex **1**, conversely, did not exhibit slow relaxation of magnetisation above 2 K. To probe the variance in the observed U_{eff} values, calculations by using CASSCF, RASSI-SO and POLY_ANISO routine were performed on these complexes to estimate the nature of the magnetic coupling and elucidate the mechanism of magnetic relaxation. Calculations gave values of $J_{Dy\text{–}Dy}$ as −1.6, 1.6 and 2.8 cm^{-1} for complexes **1**, **2** and **3**, respectively, whereas the $J_{Dy\text{–}Cr}$ interaction was estimated to be −1.8 cm^{-1} for complex **3**. The developed mechanism for magnetic relaxation revealed that replacement of the hydroxide ion by fluoride quenched the quantum tunnelling of magnetisation (QTM) significantly, and led to improved SMM properties for complex **2** compared with **1**. However, the tunnelling of magnetisation at low-lying excited states was still operational for **2**, which led to low-temperature QTM relaxation. Replacement of the diamagnetic Co^{III} ions with paramagnetic Cr^{III} led to $Cr^{III}\cdots Dy^{III}$ coupling, which resulted in quenching of QTM at low temperatures for complexes **3** and **4**. The best example was found if both Cr^{III} and fluoride were present, as seen for complex **3**, for which both factors additively quenched QTM and led to the observation of highly coercive magnetic hysteresis loops above 2 K. Herein, we propose a synthetic strategy to quench the QTM effects in lanthanide-based SMMs. Our strategy differs from existing methods, in which parameters such as magnetic coupling are difficult to control, and it is likely to have implications beyond the Dy^{III} SMMs studied herein.

Introduction

The study and development of molecule-based magnets have increased markedly over the past twenty years, with discrete molecules that exhibit a wide range of interesting physical properties, such as magnetic bistability and an enhanced magnetocaloric effect at cryogenic temperatures.[1] Discrete molecules that exhibit magnetic bistability are termed single-molecule magnets (SMMs) and are isolated as transition- or lanthanide-ion coordination complexes.[2] These molecules can store digital information by manipulating the orientation of the electrons with a magnetic field, and thus offer the potential as the ultimate high-density storage devices.[3] They rely on the creation of a large thermal barrier to magnetic reorientation (U_{eff}), which must be sufficiently higher than the thermal energy

[a] *Prof. G. Rajaraman*
Department of Chemistry, Indian Institute of Technology Bombay
Powai, Mumbai, Maharashtra, 400076 (India)
Fax: (+91) 22-2576-7152
E-mail: rajaraman@chem.iitb.ac.in

[b] *K. R. Vignesh*
IITB-Monash Research Academy, IIT Bombay
Mumbai, 400076 (India)

[c] *Dr. S. K. Langley*
School of Science and the Environment, Division of chemistry
Manchester Metropolitan University, Manchester (UK)

[d] *Prof. K. S. Murray*
School of Chemistry, Monash University Clayton
Victoria,3800 (Australia)
E-mail: Keith.Murray@monash.edu

Supporting information for this article can be found under: http://dx.doi.org/10.1002/chem.201604835.

available in the environment, otherwise no information can be stored. Below the blocking temperature (T_B; the temperature at which digital information can be stored for 100 s), SMMs act as nanomagnets, however, the highest blocking temperatures observed to date are 14 K[4] (sweep rate 0.9 mT s^{-1}) and 30 K (sweep rate 20 mT s^{-1})[5] for a radical bridged dinuclear Tb^{III} complex and a mononuclear Dy^{III} complex, respectively. Although these ultra-low temperatures are not yet viable for practical applications, ongoing research has begun to provide guidelines (synthetic and theoretical) on how to design and improve upon current materials.[6]

One suggestion is the use of lanthanide ions for the synthesis of SMMs, given that lanthanides have not been widely used until recently.[2,7] The development of lanthanide-based SMMs over the past five years has resulted in great gains in the magnitude of the thermal energy barrier (U_{eff}) and, therefore, the blocking temperature.[2b,8] A number of groups[9] have shown that the U_{eff} parameter can be "tailored" by the selection of ligands and the coordination geometry around the lanthanide ion.[10] This allows for a rational design approach that allows greater control of the properties; such designs are distinctly lacking for transition-metal-based SMMs.[2b,11] Principles have been developed to improve the thermal barrier and relaxation times of various complexes by modifying the coordination environment of the lanthanide ion in several SMMs.[12] We have recently shown this to be the case for a series of heterometallic $\{Co^{III}_2Dy^{III}_2\}$ tetranuclear complexes, in which chemical modification of the terminally coordinated ligands revealed U_{eff} values that ranged from 10 to 97 cm^{-1}.[13] Incorporation of diamagnetic elements in cluster aggregates has also been found to enhance the U_{eff} value significantly, for example, in a series of $\{Zn^{II}Dy^{III}\}$ SMMs.[10b,14]

Following on from our studies with $\{Co^{III}_2Dy^{III}_2\}$ SMM complexes,[13] which focussed on modification of the terminal ligands coordinated to the Dy^{III} ion, we have shown that the SMM properties can also easily be enhanced by the modification of a single bridging element in a heterometallic octanuclear $\{Cr^{III}_4Dy^{III}_4\}$ complex.[15] We have continued this synthetic modification approach and herein we report the molecular structures, magnetic data and theoretical characterisation of two new heterometallic 3d–4f SMM complexes with the formulae $[Co^{III}_4Dy^{III}_4(\mu\text{-OH})_4(\mu_3\text{-OMe})_4\{O_2CC(CH_3)_3\}_4(tea)_4(H_2O)_4]\cdot 4H_2O$ (**1**) and $[Co^{III}_4Dy^{III}_4(\mu\text{-F})_4(\mu_3\text{-OH})_4(o\text{-tol})_8(mdea)_4]\cdot 3H_2O\cdot EtOH\cdot MeOH$ (**2**; tea^{3-} = triply deprotonated triethanolamine, $mdea^{2-}$ = doubly deprotonated *N*-methyldiethanolamine, *o*-tol(H) = *ortho*-toluic acid). Both complexes display the same metallic topology, but importantly they are isolated with different bridging ligands (μ-OH^- vs. μ-F^-). As a consequence, we found that compounds **1** and **2** display significantly different magnetisation relaxation dynamics. We have performed in-depth ab initio and density functional theory (DFT) studies to explain these observations. To fully comprehend the role of the bridging ligand and the diamagnetic ions, we have extended our theoretical studies to the above-mentioned structurally analogous octanuclear complex, that is, $[Cr^{III}_4Dy^{III}_4(\mu\text{-F}_4)(\mu_3\text{-OMe})_{1.25}(\mu_3\text{-OH})_{2.75}(O_2CPh)_8(mdea)_4]$ (**3**), reported by us,[15] and compared the results with another structurally similar complex, $[Cr^{III}_4Dy^{III}_4(\mu_3\text{-OH})_4(\mu\text{-N}_3)_4(mdea)_4(O_2CC(CH_3)_3)_4]$ (**4**), reported by Powell and co-workers, which provided a similar F^- versus N_3^- analogy.[16]

Experimental Section

General Information

Reactions were carried out under aerobic conditions. Chemicals and solvents were obtained from commercial sources and used without further purification.

Synthesis of $[Co^{III}_4Dy^{III}_4(\mu\text{-OH})_4(\mu_3\text{-OMe})_4\{O_2CC(CH_3)_3\}_4(tea)_4(H_2O)_4]\cdot 4H_2O$ (1)

$Co(BF_4)_2\cdot 6H_2O$ (0.34 g, 1 mmol) and $Dy(NO_3)_3\cdot 6H_2O$ (0.44 g, 1 mmol) were dissolved in MeCN (20 mL), followed by the addition of triethanolamine (0.14 mL, 1 mmol), pivalic acid (0.10 g, 1.0 mmol) and triethylamine (0.55 mL, 4.0 mmol). This resulted in a dark green solution, which was stirred for 4 h. Next, the solvent was removed to give a green oil, which was re-dissolved in MeOH and layered with diethyl ether (Et_2O). Within 4–5 d, green crystals of **1** appeared (approximate yield: 34%; crystalline product). Elemental analysis calcd (%) for **1** ($Co_4Dy_4C_{48}H_{108}O_{36}N_4$): C 26.16, H 4.94, N 2.54; found: C 26.45, H 4.87, N 2.34.

Synthesis of $[Co^{III}_4Dy^{III}_4(\mu\text{-F})_4(\mu_3\text{-OH})_4(o\text{-tol})_8(mdea)_4]\cdot 3H_2O\cdot EtOH\cdot MeOH$ (2)

$Co(NO_3)_2\cdot 6H_2O$ (0.29 g, 1 mmol) and $Dy(NO_3)_3\cdot 6H_2O$ (0.44 g, 1 mmol) were dissolved in MeCN (20 mL), followed by the addition of *N*-methyldiethanolamine (0.12 mL, 1 mmol), *ortho*-toluic acid (0.13 g, 1 mmol), sodium fluoride (0.08 g, 2 mmol) and triethylamine (0.55 mL, 4.0 mmol). This resulted in a dark green solution that was stirred for 4 h. Next, the solvent was removed to give a green oil, which was re-dissolved in MeOH/EtOH (1:1) and layered with diethyl ether (Et_2O). Within 8–10 d, green crystals of **2** had appeared (approximate yield: 45%; crystalline product). Elemental analysis calcd (%) for **2** ($Co_4Dy_4C_{87}H_{120}O_{33}F_4N_4$): C 38.54, H 4.46, N 2.07, F 2.80; found: C 38.21, H 4.21, N 2.14, F 2.56.

X-ray Crystallography

X-ray measurements for **1** were performed at 123(2) K by using a Bruker Smart Apex X8 diffractometer with $Mo_{K\alpha}$ radiation. The data collection and integration were performed by using the SMART and SAINT+ software programs, and corrected for absorption by using the Bruker SADABS program. Measurements for compound **2** were performed at 100(2) K at the Australian synchrotron MX1 beamline.[17] The data collection and integration were performed by using the Blu-Ice[18] and XDS[19] software programs. Compounds **1** and **2** were solved by using direct methods (SHELXS-97)[20] and refined (SHELXL-97)[21] by using full-matrix least-squares on all F^2 data.[22] The crystallographic data and refinement parameters for **1** and **2** are summarised in Table S1. Crystallographic details are available in the Supporting Information in the CIF format. CCDC 1510015 (**1**) and 1510016 (**2**) contain the supplementary crystallographic data for this paper. These data are provided free of charge by The Cambridge Crystallographic Data Centre.

Magnetic Measurements

The magnetic susceptibility measurements were carried out by using a Quantum Design SQUID magnetometer MPMS-XL 7 operating between 1.8 and 300 K for DC-applied fields that ranged from 0–5 T. Microcrystalline samples were dispersed in Vaseline to avoid torqueing of the crystallites. The sample mulls were contained in a calibrated gelatine capsule held at the centre of a drinking straw that was fixed at the end of the sample rod. Alternating current (AC) susceptibility measurements were carried out under an oscillating AC field of 3.5 Oe and at frequencies that ranged from 0.1 to 1500 Hz.

Computational Details

By using MOLCAS 7.8,[23] ab initio calculations were performed on the Dy^{III} ions and the Cr^{III} ions by using the single-crystal structure data. The employed methodology and basis sets are described in detail in the Supporting Information. Moreover, the computed spin-orbit (SO) states have been considered in the SINGLE ANISO[24] program to compute the *g* tensors. Crystal-field parameters have been extracted by using the SINGLE ANISO code, as implemented in MOLCAS 7.8. The magnetic exchange interactions (*J*) have been computed between Dy^{III} ions (J_1) within each complex by fitting with the experimental data by using POLY ANISO.[25] The Cr–Dy (J_2) and Cr–Cr (J_3) interactions have also been computed for complex **3** (see the magnetic exchange pathways in Figure S1).

To validate the exchange coupling obtained from the POLY ANISO program further, we also computed the magnetic exchange within the density-functional formalism. The DFT calculations combined with the broken symmetry (BS) approach[26] have been employed to compute the *J* values (see the Supporting Information for details). The BS method has a proven record of giving good numerical estimates of *J* constants for a variety of coordination complexes,[27] such as dinuclear molecules,[28] Gd complexes[29] and large polynuclear complexes.[6d,27b,30]

Results and Discussion

Synthesis and Crystal Structures

Complex **1**, $[Co^{III}_4Dy^{III}_4(\mu\text{-}OH)_4(\mu_3\text{-}OMe)_4\{O_2CC(CH_3)_3\}_4(tea)_4(H_2O)_4]\cdot 4H_2O$, was synthesised by treating $Co(BF_4)_2\cdot 6H_2O$ and $Dy(NO_3)_3\cdot 6H_2O$ with triethanolamine ($teaH_3$), pivalic acid, and triethylamine in methanol. In an attempt to isolate an analogous complex with the inclusion of fluoride bridging ligands and modify the magnetic properties, we attempted a variety of reactions with various reagents and conditions. We found we could isolate one pseudo-isostructural complex with the same metallic topology, $[Co^{III}_4Dy^{III}_4(\mu\text{-}F_4)(\mu_3\text{-}OH)_4(o\text{-}tol)_8(mdea)_4]\cdot 3H_2O\cdot EtOH\cdot MeOH$ (**2**), by using NaF as a source of fluoride, with *N*-methyldiethanolamine (in place of triethanolamine), *ortho*-toluic acid (in place of pivalic acid) and acetonitrile as the solvent. Single crystals of **1** were grown from a methanolic solution, whereas a MeOH/EtOH solvent mixture was used for **2**.

Single-crystal X-ray analysis revealed that **1** and **2** are heterometallic octanuclear complexes (Figure 1, top left and right), which crystallise in the tetragonal and monoclinic space groups $I\bar{4}2m$ and $P2n$, respectively. The asymmetric unit of **1** consists of one quarter of the molecule, whereas the asymmetric unit of **2** consists of the whole molecule. The metallic-core arrangement is identical for both molecules. Each consists of four Co^{III} and four Dy^{III} ions, with an inner Dy^{III}_4 square (Dy···Dy length 3.83 Å (**1**); average Dy···Dy length 3.83 Å (**2**)) surrounded by four Co^{III}_4 ions. Each Co^{III} ion lies alternately above and below the plane of the $\{Dy_4\}$ square, capping each edge (Figure 1, bottom right; Co···Co length 6.64 Å (**1**); average Co···Co length 6.56 Å (**2**)). For comparative purposes, the molecular structure of the $\{Cr^{III}_4Dy^{III}_4\}$ analogue (**3**) is shown in Figure 1, bottom left. The valency of the Co ions were confirmed by using BVS calculations[31] and charge-balance considerations (see Tables S2 and S3 in the Supporting Information). The four Dy^{III} ions are bridged by four μ atoms and four μ_3 groups. Each μ_3 ligand also bridges to a single Co^{III} ion. The μ atoms are assigned as hydroxide (OH^-) for **1** and fluoride (F^-) for **2**. Evidence for fluoride is provided by elemental analysis and close inspection of the crystallographic data. The μ_3 bridges were found to be methoxide (MeO^-) for **1** and hydroxide (OH^-) for **2**. For both complexes, each doubly deprotonated aminepolyalcohol ligand coordinates through the N and two O atoms to an "outer" Co^{III} ion. Two O atoms then bridge from a Co^{III} to a Dy^{III} ion. For compound **1**, the third alcohol arm chelates to the Co^{III} ion, with the pivalate ligands each bridging a Co^{III} to a Dy^{III} ion. The X-ray analysis revealed disorder in the crystal for **1** (see Figure S1 and the Supporting Information). For compound **2**, however, due to the absence of the third alcohol arm, no disorder was found and eight carboxylate ligands bridge the Co^{III} and Dy^{III} ions. The four Dy^{III} ions for **1** and **2** are eight coordinate with bi-augmented trigonal prismatic geometries (see magnetic analysis below), with average Dy^{III}–L bond lengths of 2.322 and 2.334 Å, respectively. The four Co^{III} ions in **1** and **2** are six coordinate with octahedral ge-

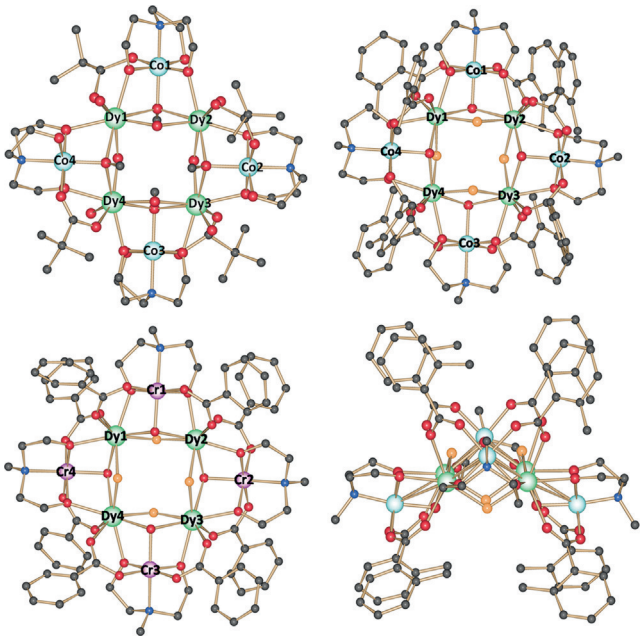

Figure 1. Molecular structures of complex **1** (top left), **2** (top right), **3** (bottom left) and a view along the plane of the $\{Dy_4\}$ square of **2** (bottom right). The disordered, solvent and H atoms were omitted for clarity. Co^{III}: light blue; Cr^{III}: pink; Dy^{III}: purple; O: red; N: blue; C: light grey; F: orange.

ometries, with average Co^{III}–L bond lengths of 1.907 and 1.908 Å, respectively. Selected bond lengths and bond angles are given in Table S4.

The key chemical features are the replacement of the hydroxide (μ-OH^-) ions in **1** by fluoride (μ-F^-) ions in **2**. We show below that this simple chemical modification impacts the magnetic properties and SMM behaviour significantly.

Magnetic Properties

DC Magnetic Susceptibility Measurements

To probe the magnetic properties, direct-current (DC) magnetic susceptibility measurements were performed on polycrystalline samples of **1** and **2** in the temperature range of 2 to 300 K by using an applied magnetic field of 1 T. The plots of $\chi_M T$ (χ_M is the molar magnetic susceptibility) versus T for **1** and **2** (Figure 2 and Figure S2) reveal room-temperature $\chi_M T$ values of 56.68 and 56.27 $cm^3 K mol^{-1}$, respectively. These values are in good agreement with the value of 56.68 $cm^3 K mol^{-1}$ expected for four Dy^{III} ions ($S=5/2$, $L=5$, $^6H_{15/2}$, $g=4/3$, $C=14.17$ $cm^3 K mol^{-1}$) that are non-interacting.[32] The four Co^{III} ions have a low-spin d^6 electronic configuration and are, therefore, diamagnetic (apart from a small second-order Zeeman contribution) and do not contribute to the magnetic susceptibility.[33] Both compounds display similar profiles, in which the $\chi_M T$ product decreased gradually between 300 and 50 K upon reduction of the temperature, owing to depopulation of the Stark sub-levels of the Dy^{III} ions due to crystal-field effects. Below 50 K, the $\chi_M T$ values fell rapidly and at 2 K reached values of 18.72 and 19.61 $cm^3 K mol^{-1}$ for **1** and **2**, respectively. These plot profiles indicate the likelihood of weak antiferromagnetic exchange interactions that occur between the Dy^{III} ions and/or a large single-ion anisotropy. The magnetic exchange interactions for **1** and **2** are discussed in detail below.

Isothermal magnetisation (M) measurements for **1** and **2**, plotted as a function of the magnetic field (H), are shown in Figure 2, bottom. The samples display similar profiles, with a rapid increase in magnetisation below 2 T before following a more gradual linear-like increase without saturation, which signifies a significant anisotropy and/or the presence of low-lying excited states. This is further supported by the magnetisation values of 21.35 and 22.01 $N\mu_B$ for **1** and **2**, respectively, at 2 K.

AC Magnetic Susceptibility Measurements

To probe for slow magnetic relaxation and SMM behaviour, the magnetisation dynamics were investigated for **1** and **2** by using alternating-current (AC) susceptibility measurements as a function of both temperature and frequency. Initially, a 3.5 Oe AC field was employed with a zero static DC field. For compound **1** (Figure 3, top left), frequency-dependent "tails" in the out-of-phase susceptibility (χ_M'') versus temperature plots were observed below 3 K, with the peak maxima falling below the operating temperature of the SQUID magnetometer. This signifies a small anisotropy barrier and/or the presence of fast QTM. In many lanthanide-containing SMMs, QTM is fast but can be quenched by the application of a static DC magnetic

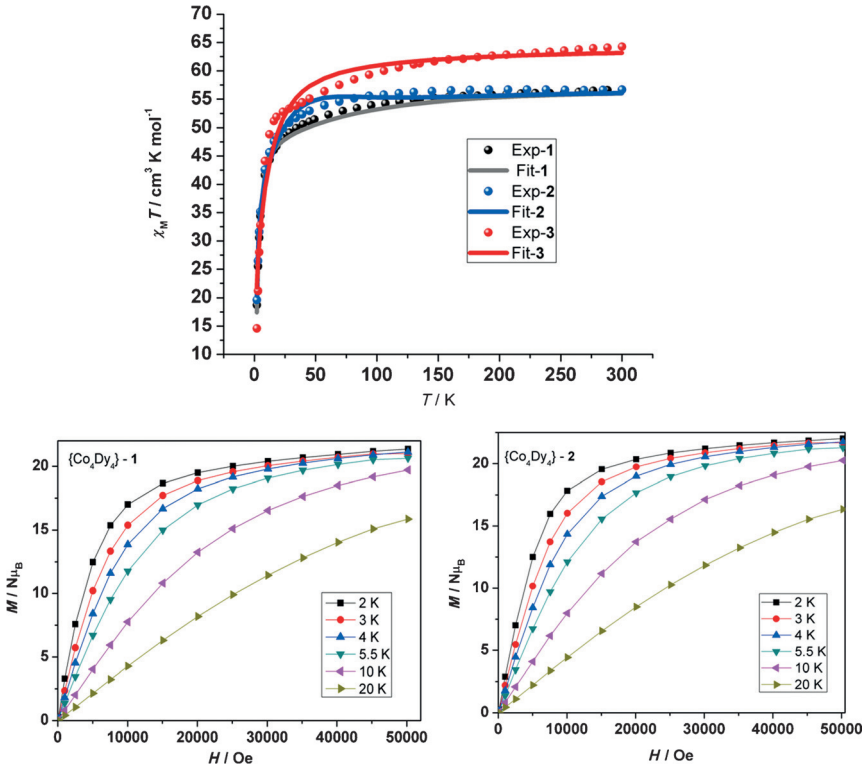

Figure 2. Top: The measured and the fitted $\chi_M T$ vs. T plots for **1**, **2** and **3** with a DC field of 1 T. Bottom: Plots of M vs. H isotherms for **1** (left) and **2** (right) at 2, 3, 4, 5.5, 10 and 20 K.

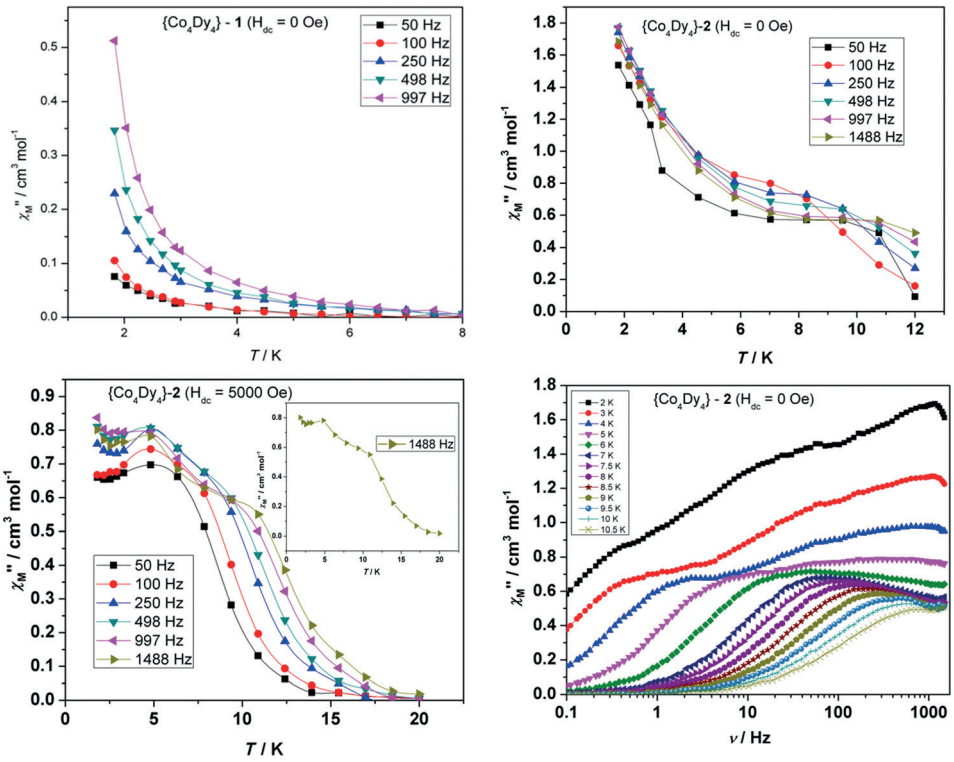

Figure 3. Top left: Plot of χ_M'' vs. T at the frequencies indicated for **1** ($H_{DC}=0$ Oe). Top right: Plot of χ_M'' vs. T at the frequencies indicated for **2** ($H_{DC}=0$ Oe). Bottom left: Plot of χ_M'' vs. T at the frequencies indicated for **2** ($H_{DC}=5000$ Oe); inset: temperature dependence of χ_M'' at 1488 Hz. Bottom right: Plot of χ_M'' vs. frequency (ν) for **2** at the temperatures indicated ($H_{DC}=0$ Oe).

field. Therefore, we probed the effect that a static magnetic field had on the relaxation time. Upon application of a 3000 Oe DC magnetic field we found that the out-of-phase signals shifted to higher temperatures, which indicated that the QTM was quenched to some extent, however, the peak maxima were obscured by a second increase at the lowest temperatures, which indicated that the QTM pathway was still active (Figure S3).

For compound **2**, however, frequency-dependent out-of-phase signals were observed below 12 K in a zero applied DC magnetic field (Figure 3, top right). An initial increase in the χ_M'' signal was found at temperatures below about 16 K, a much higher temperature than for **1** (<3 K). However, at temperatures below 6 K these signals were obscured by a larger increase in χ_M'' that did not reach a maximum above 1.8 K. This second relaxation at low temperatures is indicative of a QTM relaxation process. Due to the presence of QTM, we performed measurements in the presence of an applied DC magnetic field of 5000 Oe to quench the QTM-assisted relaxation. The χ_M'' versus T plot (Figure 3, bottom left), however, reveals a more complicated picture. It shows the likelihood of three relaxation processes, two thermally activated and one under-barrier process (QTM). This was best observed at 1488 Hz (Figure 3, bottom left, inset). At this frequency, as the temperature was reduced, peak maxima in χ_M'' were found at approximately 12 and 5 K before a further increase at the lowest temperatures. In an attempt to extract relaxation times for **2**, we performed variable-frequency (0.1–1500 Hz) studies by using a 3.5 Oe oscillating AC field at fixed temperatures (2–11 K) and with a zero static DC field. The χ_M'' versus frequency plots (Figure 3, bottom right), as expected, reveal multiple relaxation pathways, of which at least three are identifiable. This is evident at the lowest temperatures (2–5 K) and from the Cole–Cole plots (χ_M' vs. χ_M'', Figure 4, inset) which reveal several fused semi-circular profiles. From the obtained data, it is possible to extract/extrapolate relaxation times for the slowest process (the χ_M'' peak maximum that correspond to the lowest frequency at a fixed temperature). For this process, the susceptibility maxima are dependent on temperature, which indicates a thermally activated relaxation mechanism at the temperatures probed. Plots of $\ln(\tau)$ versus $1/T$ are linear between 8 and 10.5 K (Figure 4). However, below 7 K the relaxation times deviate from linearity (Figure S4). This confirms that a thermally activated Orbach process operates at higher temperatures and the low-temperature deviation suggests a crossover towards a QTM relaxation mechanism. Fitting the data to the Arrhenius law ($\tau=\tau_o\exp(U_{eff}/k_BT)$) in the linear (thermally activated) region gave a significant effective anisotropy barrier to magnetisation reversal of $U_{eff}=(39\pm1)\ cm^{-1}$ with $\tau_o=1.0\times10^{-6}$ s ($R=0.99$). Relaxation data for the second and third processes could not be extracted from the data collected.

A comparison of compounds **1** and **2** reveal strikingly different magnetisation dynamics. For **1** ($H_{DC}=0$ Oe), no maxima in the χ_M'' signals were observed above 2 K, whereas maxima (multiple relaxation pathways at the lowest temperatures) were found for compound **2** up to 12 K. In essence, we ob-

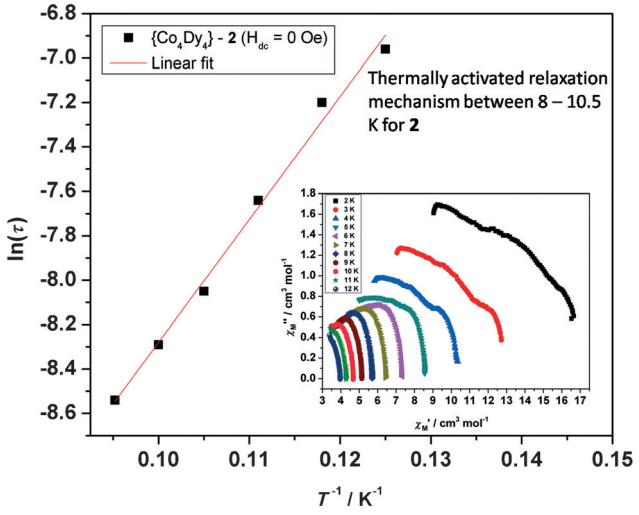

Figure 4. Magnetisation relaxation time (τ) plotted as ln(τ) vs. T^{-1} for compound **2**. The solid red line represents a fit to the Arrhenius law in the thermally activated regime. Inset: Cole–Cole plots of **2** at temperatures between 2 and 12 K.

served a significant increase in the magnetic relaxation time at the temperatures probed for compound **2**. This observation is important because the difference between the two molecules is minor and consists of a small chemical modification of the first coordination sphere of the Dy^{III} ions, that is, the substitution of the bridging μ-OH ions for the μ-F ions. This strongly suggests that chemical modification of existing complexes, which are predominantly oxo-based, can result in longer relaxation times and, therefore, SMMs with relatively better performance.

A similar situation was recently reported for two analogous heterometallic octanuclear $\{Cr^{III}_4Dy^{III}_4\}$ complexes (**3** and **4**).[15–16] The metallic core topology of **3** and **4** is identical to that found for **1** and **2** (Figure 1). The magnetic measurements revealed that complex **4** displays SMM behaviour with relatively fast relaxation times at about 2 K, whereas after modification of the bridging ligands, that is, the replacement of N_3^- (**4**) by F-donor ligands (**3**), a significant increase in relaxation time was observed for **3**, when compared at the same temperature. It was reported that **4** displayed a U_{eff} value of 10.4 cm^{-1}, whereas the U_{eff} value for **3** was 55.0 cm^{-1}. More interestingly, the relaxation time for **3** was long enough to observe highly coercive magnetic hysteresis loops at temperatures below 3.5 K (Figure S5).[15] With these results in mind, it is important to elucidate the factors that are responsible for the observation of longer relaxation times (at a particular temperature) in near-identical complexes. Therefore, we have performed ab initio calculations on the two $\{Co^{III}_4Dy^{III}_4\}$ complexes (**1** and **2**) to determine these factors. We have also performed a theoretical analysis on $\{Cr^{III}_4Dy^{III}_4\}$ analogue **3** and compared the data with previously reported results for complex **4**.

Theoretical Studies

The magnetic properties of **1**, **2** and **3** have been studied theoretically by using ab initio CASSCF + RASSI-SO calculations. The SINGLE_ANISO routine was used to compute the anisotropy of the individual Dy^{III} and Cr^{III} ions and POLY_ANISO was used to employ the Lines model to fit the susceptibility/temperature plots. First we discuss the magnetic anisotropy at the single Dy^{III} ion level and the corresponding single-ion relaxation mechanism. We then expand the discussion to include the exchange coupling between the $Dy^{III}\cdots Dy^{III}$ and $Cr^{III}\cdots Dy^{III}$ ions for **1**–**3** and develop a new exchange-coupled relaxation mechanism, which was found to be in good agreement with the experimental data.

Mechanism of Magnetic Relaxation: Single-Ion Paradigm

Because the Co^{III} ions in **1** and **2** are diamagnetic, the SMM behaviour originates from the Dy^{III} anisotropy alone. Thus we have explored the anisotropy of Dy^{III} for all four centres in **1** and **2** by using ab initio methods. In compound **3**, conversely, we explored the anisotropy of all the ions (Cr^{III} and Dy^{III}). Analysis of the coordination environment of each Dy^{III} ion for **1**–**4**, by using the SHAPE program,[34] revealed there are two types of non-equivalent Dy^{III} sites in **1**–**3** (Dy1 and Dy2, Figure 1), whereas in **4** all Dy^{III} ions are equivalent. The geometry of each Dy^{III} ion in **1**–**3** is best described as a bi-augmented trigonal prism. A deviation with respect to an ideal bi-augmented trigonal prism of 0.6, 1.3 and 1.07 for (Dy1 and Dy4) and 0.8, 1.0 and 1.05 for (Dy2 and Dy3) was found for **1**, **2** and **3**, respectively. For compound **4**, all Dy^{III} ions were found in a square anti-prismatic geometry. A deviation of 0.5 for each Dy^{III} ion was observed with respect to an ideal square anti-prismatic geometry. To fully understand the single-ion relaxation process, we undertook CASSCF + RASSI-SO calculations to compute the anisotropy of the individual Dy^{III} ions by using MOLCAS 7.8 (see the Supporting Information for computational details). The calculated anisotropic g values are listed in Table 1 and Tables S6, S9 and S13, and their anisotropy orientations are shown in Figure 5. It was found that sites (Dy1, Dy4) and (Dy2, Dy3) possess similar anisotropic parameters (see Table 1), as a reflection of the SHAPE analysis. The computed energies of the eight low-lying Kramer's doublets (KDs) also reflect that there are two types of Dy^{III} ions for **1**–**3** (see Tables S5, S8 and S11). The energy gap between the ground and

Table 1. Ab initio-computed ground-state g tensors for each Dy^{III} centre in **1**–**4**.

Complex	Tensor	Dy1	Dy2	Dy3	Dy4
1	g_x	0.9705	0.5419	0.5806	0.1004
	g_y	6.6958	1.8736	2.1638	6.3070
	g_z	13.3107	18.0245	17.7693	13.4578
2	g_x	0.0098	0.0039	0.0028	0.0009
	g_y	0.2842	0.0576	0.0360	0.2142
	g_z	19.4753	19.6320	19.6578	19.3850
3	g_x	0.0626	0.1995	0.1862	0.0653
	g_y	0.1349	1.0026	0.9827	0.1426
	g_z	19.6892	18.0941	18.0411	19.5603
4	g_x	1.6671			
	g_y	5.8397			
	g_z	14.4193			

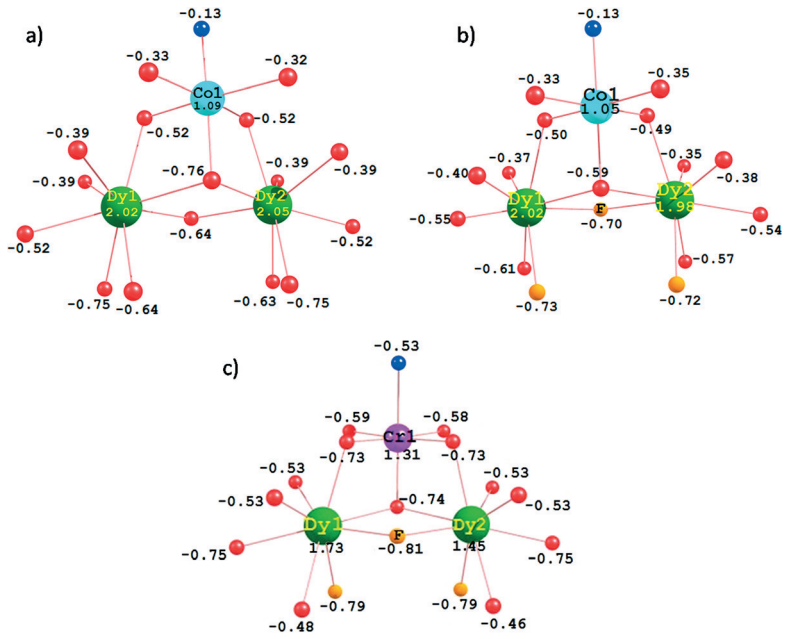

Figure 5. DFT-computed Mulliken charges on the donor atoms of a) **1**, b) **2** and c) **3**.

the first excited state KDs were found to be 4.9 (Dy1) and 8.4 cm^{-1} (Dy2) in **1**, 42.9 (Dy1) and 68.9 cm^{-1} (Dy2) in **2**, and 40.6 (Dy1) and 25.6 cm^{-1} (Dy2) in **3**. For compound **4**, with only one equivalent Dy^{III} ion, the gap between the ground and first excited state was reported to be 23.3 cm^{-1}.[16] These results show that the energy gap between the ground and first excited state was significantly larger for complexes **2** and **3** than for complex **1**. Complex **4** is intermediate. Because the energy gap is correlated to the crystal-field-splitting energy, this suggests relatively weaker splitting of the m_J levels in **1** compared with **2**–**4**.

For complex **1**, all the Dy–O bonds are in the range of 2.32 to 2.44 Å except for the Dy–O(H) bonds, which are shorter (2.22 Å). Because the μ-OH ligands are bridging between Dy^{III} ions and because of the square $\{Dy^{III}_4\}$ topology, they lie at right angles to each other at the Dy^{III} site. These hydroxide bridges were found to have large negative Mulliken charges that force the β-electron (spin-down) of the Dy^{III} ion to lie perpendicular to these bridges to minimise electrostatic repulsion (see Figure 5a). This forces the g_{zz} axis to be perpendicular to the β-electron density, that is, it lies along one of the Dy–OH axes (see Figure 6a). The proximity of the diamagnetic Co^{III} ion to the two a μ_3 alkoxide bridges enhances the negative charge on these oxygen atoms because a strong polarisation from a +3 cation is expected. Therefore, these methoxide bridges have very large negative charges compared with the hydroxide bridges (see Figure 5a), which further forces the g_{zz} axis to lie along the hydroxide bridge. The magnetic anisotropy of the oblate Dy^{III} ion arises due to crystal-field splitting of the m_J levels because this is correlated to the nature of the interactions. Although a stronger axial interaction is exerted by the hydroxide, which ensures stabilisation of $m_J = \pm 15/2$ as the ground state, because the two hydroxide bridges are at right angles to each other, this results in the stabilisation of $m_J = \pm 1/2$ as the first excited state. The minor variation in the energy gaps between the ground and first excited state for Dy1 and Dy2 is due to minor structural alterations, as described by the SHAPE analysis.

In complex **2** the bridging hydroxide (μ-OH^-) ligands were replaced by fluoride (μ-F^-) ions. The Dy^{III}–O bonds found in complex **2** are very similar to those of complex **1**. The average Dy^{III}–F bonds were found to be 2.247 Å. Each fluoride ion was found to possess a strong negative charge, which forces g_{zz} to

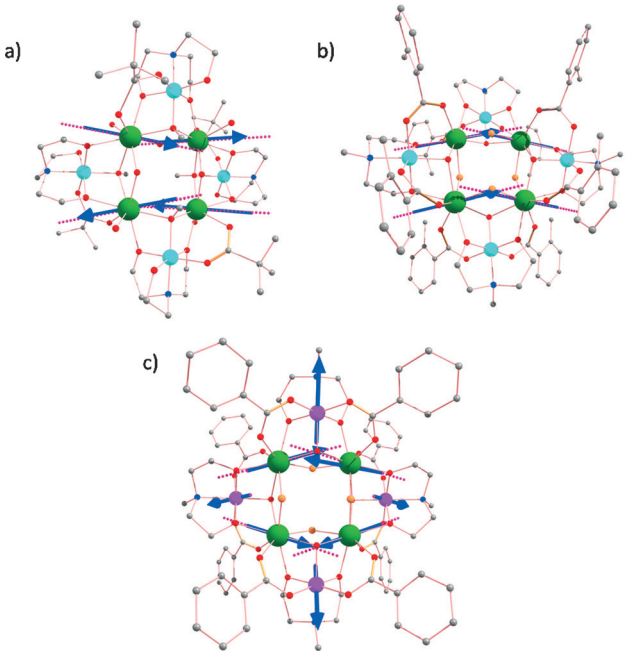

Figure 6. The directions of the local anisotropy axes in the ground KDs on each Dy^{III} site (blue arrows) in a) **1**, b) **2** and c) **3**, along with the anisotropy axes of Cr^{III} ions in **3** (c).

lie along the Dy^{III}–F bond (see Figure 6b). As explained above, because two fluoride ions are bonded to the Dy^{III} ion at right angles to each other, $m_J = \pm 1/2$ is stabilised as the first excited state. Because the fluoride ion is a harder base than hydroxide, it exerts a stronger electrostatic repulsion and, therefore, pushes the first excited state higher in energy by 42.9 and 37.7 cm^{-1} for Dy1 and Dy2, respectively, compared with **1**. Another important reason for the larger gap in **2** than in **1** is due to the smaller negative charge found on the bridging oxygen atom that connects the two Dy^{III} ions (see Figure 5b). In complex **1**, these are alkoxide bridges which provide a significantly larger negative charge on the equatorial plane (see Figure 5a), whereas in complex **2** the hydroxide ions reduce this repulsion considerably. Complex **3** has hydroxide (μ_3-OH^-) and alkoxide (μ-O-mdea) O atoms, which possess very large negative charges (see Figure 5c), *trans* to each other; this favours the arrangement of the g_{zz} axis along this axis (see Figure 6c) and leads to a larger ground–first excited state gap than complex **1**.

The computed *g* anisotropies of **1**–**4** are given in Table 1. In all cases, $m_J = \pm 15/2$ was found to be stabilised as the ground state because the axial interactions are stronger than the equatorial interactions. However, in complex **1** a significant transverse anisotropy was present for the ground-state KD due to the strong mixing of $m_J = \pm 15/2$ and $\pm 1/2$ states (see Figure 7a and b). A similar situation was encountered for **4**.[16] The transverse component for the Dy2 and Dy3 ions were considerably less than Dy1 and Dy4 due to the larger energy gap between the $m_J = \pm 15/2$ and $\pm 1/2$ states.

Due to the significant transverse anisotropy and the low-lying first excited state of **1**, it was not expected to exhibit a magnetisation blockade at the single-ion level, as revealed from experiment. For complexes **2** and **3**, conversely, the g_z values were almost purely axial in nature. This is because the mixing of the $m_J = \pm 15/2$ state with the excited states was significantly reduced due to the increased energy gap between the ground KD and the excited-state KD. More importantly, because the first-excited-state KD was significantly higher in energy, this suggests a possible magnetisation blockade at the single-ion level.[35]

To determine the relaxation processes associated with single-ion Dy^{III} anisotropy, the mechanisms of magnetic relaxation were computed and are shown in Figure 7. In complex **1**,

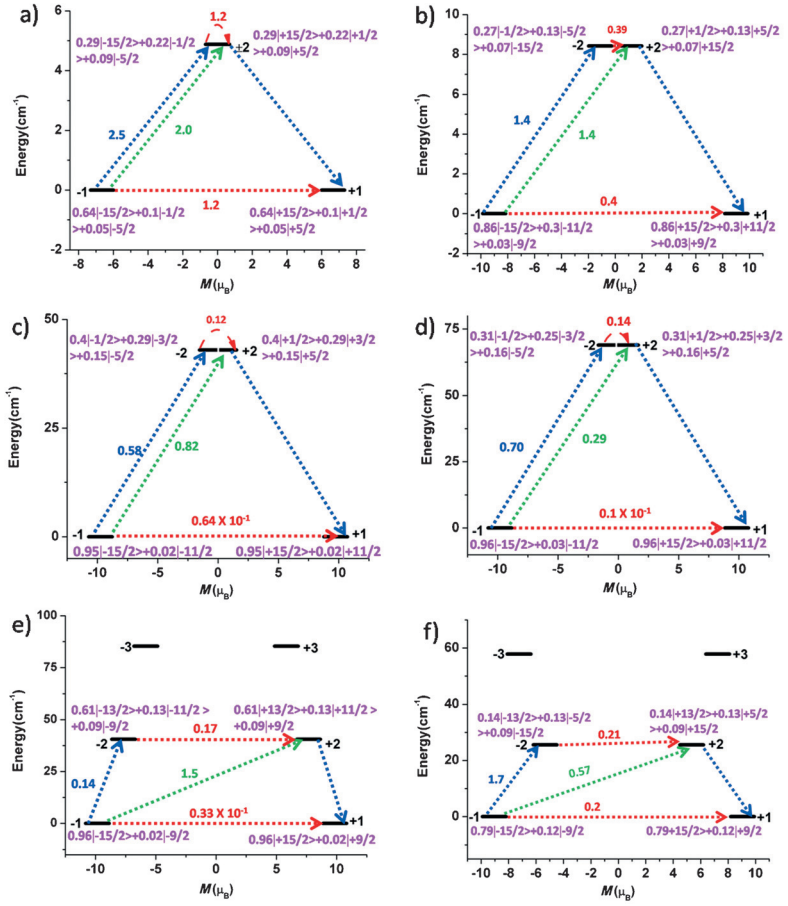

Figure 7. The ab initio-computed magnetisation blocking barrier for a) the Dy1 site in **1**; b) the Dy2 site in **1**; c) the Dy1 site in **2**; d) the Dy2 site in **2**; e) the Dy1 site in **3** and f) the Dy2 site in **3**. The *x* axis indicates the magnetic moment of each state along the main magnetic axis of the Dy ions, whereas the *y* axis denotes the energy of the respective states. The thick black line indicates the KDs as a function of the computed magnetic moment. The green/blue arrows show the possible pathway by Orbach/Raman relaxation. The dotted red lines represent the presence of QTM/TA-QTM between the connecting pairs. The numbers provided at each arrow are the mean absolute value for the corresponding matrix element of the transition magnetic moment. The numbers in magenta correspond to wavefunction analysis of the m_J levels, in which, for example, $0.95\,|{-15/2}> + 0.02\,|{-9/2}>$ indicates that the ground state is pure $m_J = \pm 15/2$ with slight mixing (0.02) with an $m_J = 9/2$ excited state.

the ground-state tunnelling probability is large for all Dy^{III} ions, which as expected leads to no magnetisation blockade (see Figure 7a and b). However, in complex **2** the ground-state tunnelling probability is smaller than **1** (0.64×10^{-1} and 0.1×10^{-1} μ_B), but not sufficiently negligible to quench the QTM completely at the ground-state level. That is, if an isostructural $\{Co^{III}_4Dy^{III}La^{III}_3\}$ complex is prepared, it is unlikely to show SMM behaviour due to the large ground-state tunnelling probability (see Figure 7c and d). However, if we consider relaxation beyond a single-ion mechanism, factors such as $Dy^{III}\cdots Dy^{III}$ exchange coupling could quench the observed QTM effects and lead to a possible magnetisation blockade (see below). In complex **3**, the tunnelling probability at the single-ion level is larger than in **2**, and the calculations again predict the absence of SMM behaviour (see Figure 7e and f). This is, however, contrary to what was observed in the experimental measurements.[15] To explain the data, we must take into account the $Dy^{III}\cdots Dy^{III}$ and $Cr^{III}\cdots Dy^{III}$ exchange coupling. CASSCF calculations performed for the Cr^{III} single ions gave isotropic *g* tensors (see Table S13 in the Supporting Information) and axial zero-field splitting parameter values of -0.2 cm^{-1} for Cr1 and -0.3 cm^{-1} for Cr2, Cr3 and Cr4, with a small *E/D* ratio. These values are too small to significantly influence the magnetic anisotropy of the Dy^{III} centres.

Mechanism of Magnetic Relaxation: Polynuclear Paradigm

As illustrated above, the single-ion Dy^{III} anisotropy and the developed mechanism of relaxation does not rationalise the observation of slow magnetic relaxation in complexes **1**–**3**. To gain insight into the mechanism of relaxation, a polynuclear mechanism needs to be developed that incorporates the exchange coupling between the paramagnetic centres. This has been performed by using the POLY ANISO program with the Lines model to fit the susceptibility data by using the ab initio-computed parameters of the Dy^{III}/Cr^{III} single ion. This has successfully been employed to extract a good numerical estimate of the magnetic exchange parameters (*J* values) in several earlier instances.[13e,f,36] The exchange Hamiltonian adopted for complexes **1**, **2** and **3** is given below [Eq. (1)], along with the exchange topology diagram shown in Figure 8.

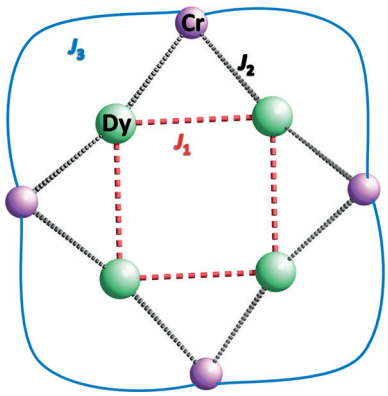

Figure 8. Magnetic exchange pathways in **1**–**3**. Cr replaced by Co in **1** and **2**.

$$\hat{H}_{ex} = -\sum_{i=1}^{3} J_i S_i S_{i+1} \quad (1)$$

in which $J_i = J_i^{exch}$; that is, J_i are the fitted J_i^{exch} parameters; this describes the interaction between all the neighbouring metal centres.

Due to the high symmetry found in complexes **1** and **2**, the Dy^{III}-O-Dy^{III} and Dy^{III}-F-Dy^{III} angles are identical for all Dy^{III}–Dy^{III} pairs. Therefore, we have employed a single exchange interaction (J_1) for these two complexes. For complex **3**, two additional magnetic exchange parameters, Dy^{III}–Cr^{III} (J_2) and Cr^{III}–Cr^{III} (J_3), were employed (see the Computational Details and Figure 8).[16,37]

Although the Cr^{III}–Cr^{III} (J_3) exchange is a next-nearest-neighbour interaction, this interaction has previously been highlighted as being important to reproduce the low-temperature susceptibility data and, therefore, has been taken into consideration.[38]

The estimated exchange coupling parameters for complexes **1**–**3** are shown in Table 2 (see Figure 2 for the fit obtained by using the POLY ANISO routine). For complex **1**, the Dy^{III}–Dy^{III} magnetic exchange interaction was found to be antiferromagnetic (-0.16 cm^{-1}) in nature. The average Dy^{III}-O-Dy^{III} angle in complex **1** is 111.3°. Based on previously developed magneto-structural correlations for $\{Gd^{III}(OR)_2Gd^{III}\}$ dimers, this angle falls in the antiferromagnetic exchange region.[29b] DFT calculations also reproduced the sign of the exchange interaction, which confirmed this point. For complex **2**, the POLY ANISO fit gave a ferromagnetic coupling interaction (1.6 cm^{-1}). Here, the average Dy^{III}-O-Dy^{III} angle was found to be 107.8°, whereas the average Dy^{III}-F-Dy^{III} angle was 113.8°. The above-mentioned magneto-structural correlation predicted ferromagnetic exchange coupling for angles below approximately 107°, and this is consistent with the present observation. The magnitude of the exchange interaction, however, is relatively strong compared with other 4f–4f interactions (usually <0.01 cm^{-1}) and this can be traced to the presence of the fluoride bridges, which promote strong polarisation (see Figure S6 in the Supporting Information).

For complex **3**, the J_1 interaction between the Dy^{III}–Dy^{III} ions was found to be ferromagnetic, as observed in **2**. In this case the exchange was even stronger, with a magnitude of 2.8 cm^{-1}. The average Dy^{III}-O-Dy^{III} angle was found to be 105.5°, whereas the average Dy^{III}-F-Dy^{III} angle was 118.5°. Relative to the $\{Gd(OR)_2Gd\}$ magneto-structural correlation, the stronger Dy^{III}-O-Dy^{III} magnetic exchange coupling witnessed in

Table 2. Magnetic exchange interactions between magnetic ions in **1**–**3**; *zJ* is a cluster–cluster interaction.

Complex	Magnetic exchange interactions						
	Lines model [cm^{-1}]				DFT calculated [cm^{-1}]		
	J_1	J_2	J_3	zJ	J_1	J_2	J_3
1	−0.16			−0.01	−0.11		
2	1.6			−0.013	0.034		
3	2.8	−1.8	0.005	−0.017	0.02	−0.8	0.005

3 is correlated to a smaller Dy^{III}-O-Dy^{III} angle compared to **2**. Furthermore, because the Dy^{III}–Cr^{III} interaction was determined to be antiferromagnetic, this offers another route for stronger ferromagnetic Dy^{III}···Dy^{III} coupling through spin polarisation, as shown earlier for polynuclear {3d-Gd} complexes.[38]

The Dy^{III}–Cr^{III} interaction was estimated to be antiferromagnetic in nature ($-1.8\ cm^{-1}$ by using POLY ANISO and $-0.8\ cm^{-1}$ by using DFT, based on {$Cr^{III}Gd^{III}$} models). We have previously undertaken detailed mechanistic studies on {3d$(OR)_2$Gd} pairs and fluoride-bridged {Cr^{III}-Gd^{III}} pairs.[39] Conclusions from this work are that the magnetic exchange coupling in {3d–4f} pairs has two contributions. A ferromagnetic contribution arises from the charge transfer from a 3d orbital to empty 5d/6s orbitals of Dy^{III} with the Dy^{III} 4f orbitals contributing to the empty 5d/6s orbitals through polarisation, as discussed earlier.[38b] The second contribution is an antiferromagnetic contribution that results from the direct overlap between the 3d SOMOs and the 4f SOMOs.

In general, unpaired electrons in σ-type d_{z^2} and $d_{x^2-y^2}$ orbitals contribute significantly to charge transfer, which leads to dominating ferromagnetic contributions, whereas the remaining π orbitals tend to overlap with the 4f orbitals. In the case of Cr^{III}, which has the t_{2g}^3 configuration, the charge-transfer pathway was negligible and significant overlap with the 4f orbitals is expected, and is therefore an antiferromagnetic interaction.[6c,39] In complex **3**, the Dy^{III}–Cr^{III} interaction is mediated by two alkoxide bridges and one carboxylate bridge. Extensive magneto-structural correlations developed for {$Cu^{II}Gd^{III}$},[40] {$Ni^{II}Gd^{III}$},[38] {$V^{IV}Gd^{III}$},[41] {$Cr^{III}Gd^{III}$}[29b,39] and {$Fe^{III}Gd^{III}$}[6c,42] complexes suggest that, for this exchange topology, the coupling was expected to be antiferromagnetic for bridge angles smaller than 105°. Here, the Dy^{III}-O-Cr^{III} angles were 103.4 and 98.4°. These relatively small angles enforced in the polynuclear framework therefore promoted antiferromagnetic coupling, and this was expected to be relatively strong because one of the prominent ferromagnetic contributions is negligible, as discussed above. These mechanistic arguments are supported by the DFT calculations (see Figure S6).

Magnetic Relaxation in the Polynuclear Framework

For compound **1**, the tunnelling parameter (Δ_{tun}) for the exchanged coupled ground state was computed to be large ($2.4\times10^{-3}\ cm^{-1}$, see Figure 9a), but was determined to be very small for **2** ($4.4\times10^{-6}\ cm^{-1}$, see Figure 9c) and **3** ($4.0\times10^{-7}\ cm^{-1}$, see Figure 9b). Thus, in complex **1** the magnetic relaxation occurs via the ground state with a small energy barrier of $0.001\ cm^{-1}$ (see Table S6 and Figure 9a). In complex **2**, the first excited state also possesses negligible tunnel splitting, which suggests a magnetisation blockade of up to $3.6\ cm^{-1}$. The second excited exchange-coupled state lies at $4.0\ cm^{-1}$ (see Table S10 and Figure 9c) and possesses a tunnel splitting of $\Delta_{tun}=2.8\times10^{-4}\ cm^{-1}$, which suggested a possible relaxation pathway via this state. Furthermore, another relaxation pathway at higher excited states was expected with an energy barrier of $49.1\ cm^{-1}$ and with significant tunnel splitting ($\Delta_{tun}=1.1\times10^{-5}\ cm^{-1}$, see Table S10). Although the relaxation was expected to occur via the states that lie at $4.0\ cm^{-1}$, the tunnel splittings for these states were relatively small and minor perturbations, such as intermolecular interactions, can quench this tunnelling process and could push up the relaxation barrier via higher excited states at $49.1\ cm^{-1}$. This picture is consistent

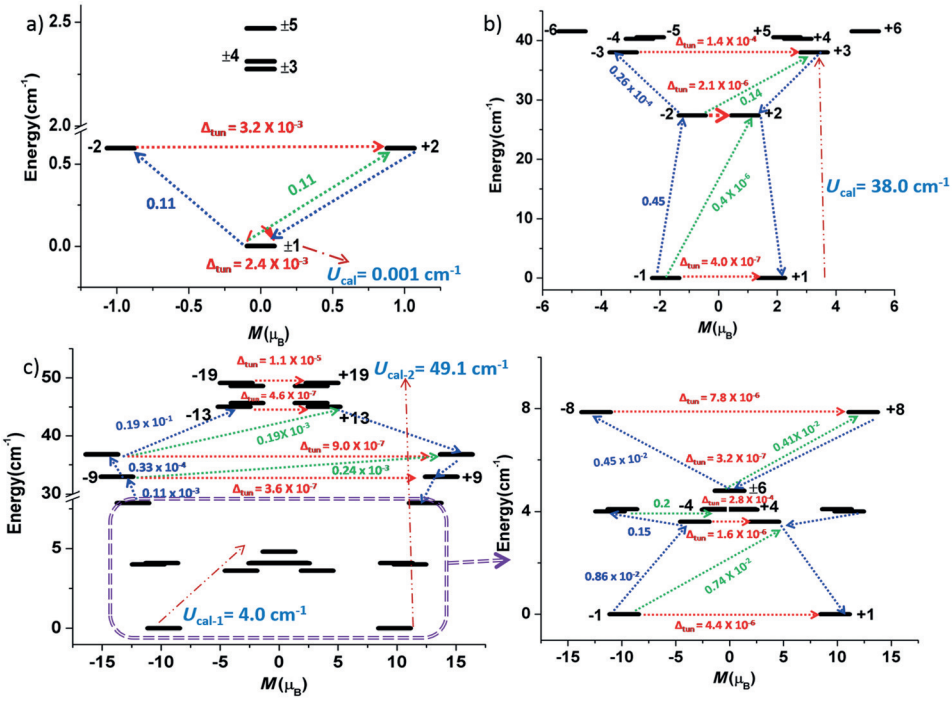

Figure 9. Low-lying exchange spectrum and the position of the magnetisation blocking barrier for a) **1**, b) **3** and c) **2**. The exchange states are placed on the diagram according to their magnetic moments (bold black lines).

with the experimental data in which several relaxation processes were observed, one at very low temperatures with a small barrier height (2–4 cm^{-1}, estimated) and one at higher temperatures with a barrier height of 39 cm^{-1} (experimental).

In contrast, for **3** the tunnelling probabilities of the ground, first and second excited states were almost negligible, a consequence of stronger Dy^{III}···Dy^{III} and Cr^{III}···Dy^{III} interactions that quenched the QTM and led to relaxation via the third exited state. This places the estimate of U_{cal} for this molecule at 38.0 cm^{-1} ($\Delta_{tun} = 1.4 \times 10^{-4}$ cm^{-1}, see Table S14 and Figure 9b), which is consistent with the experimental data (55 cm^{-1}).[15] Clearly, unlike **2** only one relaxation was observed here, which suggests that the presence of Cr^{III} ions have therefore quenched the low-temperature relaxation channel that was available for complex **2**.

The barrier heights for magnetisation reversal were found to be **1** (0.001 cm^{-1}) < **2** (4.0 cm^{-1}) < **4** (10.4 cm^{-1}) < **3** (38.0 cm^{-1}).[43] The observed trend clearly suggests that the presence of F^- ions (**2** (F^-) vs. **1** (OH^-) and **3** (F^-) vs. **4** (N_3^-)) instigated structural and electronic changes that helped to quench the QTM to a certain extent. This is clear if we compare complexes **1** and **2**; **1** is experimentally not an SMM, whereas complex **2** exhibited slow relaxation, but with prominent QTM at lower temperatures. Although the F^- ions helped to quench the tunnelling compared with the hydroxide ions present in **1**, we still found a significant tunnel splitting of the exchanged coupled excited state in complex **2** (2.8×10^{-4} cm^{-1}). Complex **4**, however, incorporates the paramagnetic Cr^{III} ion, which induced notable exchange coupling between the Cr^{III}–Dy^{III} and Dy^{III}–Dy^{III} ions and quenched the QTM effects. Here, even with bridging hydroxide and azide ligands, QTM was quenched efficiently. This was attributed to the relatively strong Dy^{III}–Cr^{III} magnetic exchange interactions. Additionally, if both F^- and Cr^{III} are present, such as in complex **3**, this was doubly effective and both factors worked additively to quench the QTM and led to the observation of a very large barrier for magnetisation reversal, which ultimately resulted in coercive magnetic hysteresis loops with a blocking temperature of 3.5 K (Figure S5). Our calculations revealed that the electrostatic potential experienced by the ions upon replacement of OH^- by F^- is significant and alters the direction of the ground-state magnetic anisotropy. Because the F^- ions carry a larger negative charge compared with the hydroxide ions, the barrier heights were also found to correlate to the computed Mulliken charges that reside on the bridging atoms (see Figure 10 and Tables S15–S17 and Figures S7–S9 in the Supporting Information).

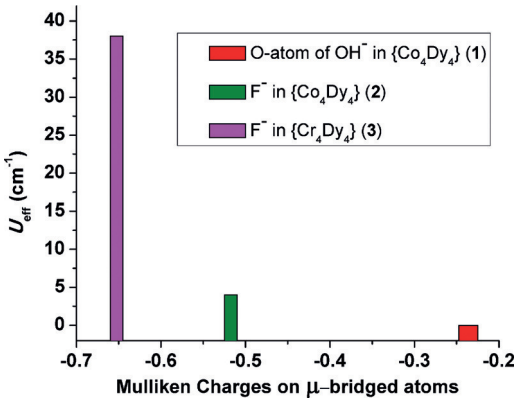

Figure 10. Plot of observed U_{eff} values in {$TM^{III}_4Dy^{III}_4$} vs. Mulliken charge on bridged atoms.

Conclusion

In summary, we report the synthesis and magnetic and theoretical studies of two analogous heterometallic {$Co^{III}_4Dy^{III}_4$} octanuclear complexes. Both complexes display the same metallic core topology with minor structural modifications found in the ligand framework. The major structural difference, in the context of the magnetic behaviour, is the introduction of μ-F^- bridging ions for **2** that replace the μ-OH^- ions in **1**. We also reported a theoretical perspective of two analogous {$Cr^{III}_4Dy^{III}_4$} octanuclear complexes (**3** and **4**), which displays a metallic core topology identical to that of **1** and **2**. Compounds **3** and **4** provided a similar O versus F bridging ligand comparison to **1** and **2** (i.e. N vs. F), but also revealed insight into the influence of the 3d transition-metal ion on the magnetic behaviour on comparing **1** and **2** to **3** and **4**. The magnetic relaxation data for **1** and **2** (TM = Co^{III}) were found to be significantly different, as were the data for **3** and **4** (TM = Cr^{III}). Furthermore, the behaviour of the {$Co^{III}_4Dy^{III}_4$} complexes was notably different from the {$Cr^{III}_4Dy^{III}_4$} complexes. From the AC data, only out-of-phase (χ_M'') tails were visible above 2 K for **1**. However, complex **2** exhibited a significant out-of-phase component that revealed multiple relaxation processes, the slowest of which had a barrier height of 39 cm^{-1}.

Ab initio calculations suggested that major differences were found even at the single-ion level, in which the presence of F^- was found to diminish the tunnelling probability of the ground-state KDs. In the hydroxide-bridged complexes, the ground-state tunnelling was significantly larger and we showed that compounds **1** and **4** are "worse" SMMs than **2** and **3**. The presence of the F^- ions altered the direction of the magnetic anisotropy and, more importantly, pushed the first excited state higher in energy due to stronger electrostatic repulsion. This reduced the mixing of the ground $m_J = 15/2$ state with the first excited $m_J = 1/2$ state and led to reduced QTM effects for the F^- compounds.

At the polynuclear level, the presence of weak Dy^{III}–Dy^{III} interactions was already strong enough to quench the QTM completely in complex **2**, which led to the observation of SMM behaviour, whereas it was insufficient in complex **1**, which showed no SMM characteristics. Furthermore, F^- also influenced the exchange coupling, in which the Dy^{III}–Dy^{III} coupling was determined to be ten times larger for complex **2** than for complex **1** (−0.16 cm^{-1} vs. 1.6 cm^{-1} for **1** and **2**, respectively), which further reiterated the superiority of F^- over OH^- as a bridging ligand.

Replacement of (diamagnetic) Co^{III} by the paramagnetic d^3 Cr^{III} ion opened up further exchange pathways, for which stronger Dy^{III}···Cr^{III} interactions were detected and led to further

quenching of the QTM pathways. This was particularly the case in complex **3**, in which both Cr^{III} and F^- are present and both factors contributed additively to the quenching of QTM, which led to the observation of a very large barrier height for magnetisation reversal and long relaxation times, as observed in the magnetic hysteresis plot.

Acknowledgements

K.S.M. thanks the Australian Research Council (ARC) and K.S.M. and G.R. thank the Australia–India Strategic Research Fund (AISRF) for support of this work. K.R.V. is thankful to the IITB-Monash Research Academy for a PhD studentship. The authors thank Dr Boujemaa Moubaraki for help with magnetism. Structural aspects of this research were undertaken on the MX1 beamline at the Australian Synchrotron, Clayton, Victoria, Australia.

Keywords: bridging ligands · exchange interactions · lanthanides · magnetic properties · quantum chemistry

[1] a) R. Sessoli, D. Gatteschi, A. Caneschi, M. A. Novak, *Nature* **1993**, *365*, 141 – 143; b) M. Evangelisti, E. K. Brechin, *Dalton Trans.* **2010**, *39*, 4672 – 4676.

[2] a) R. A. Layfield, *Organometallics* **2014**, *33*, 1084 – 1099; b) D. N. Woodruff, R. E. P. Winpenny, R. A. Layfield, *Chem. Rev.* **2013**, *113*, 5110 – 5148; c) P. Zhang, Y.-N. Guo, J. Tang, *Coord. Chem. Rev.* **2013**, *257*, 1728 – 1763.

[3] a) D. Gatteschi, R. Sessoli, J. Villain, *Molecular Nanomagnets*, Oxford University Press, Oxford, **2006**; b) D. Gatteschi, *Adv. Mater.* **1994**, *6*, 635 – 645.

[4] a) J. D. Rinehart, M. Fang, W. J. Evans, J. R. Long, *J. Am. Chem. Soc.* **2011**, *133*, 14236 – 14239; b) J. D. Rinehart, M. Fang, W. J. Evans, J. R. Long, *Nat. Chem.* **2011**, *3*, 538 – 542.

[5] S. K. Gupta, T. Rajeshkumar, G. Rajaraman, R. Murugavel, *Chem. Sci.* **2016**, *7*, 5181 – 5191.

[6] a) N. F. Chilton, *Inorg. Chem.* **2015**, *54*, 2097 – 2099; b) S. Sanz, J. M. Frost, T. Rajeshkumar, S. J. Dalgarno, G. Rajaraman, W. Wernsdorfer, J. Schnack, P. J. Lusby, E. K. Brechin, *Chem. Eur. J.* **2014**, *20*, 3010 – 3013; c) K. S. Pedersen, G. Lorusso, J. J. Morales, T. Weyhermüller, S. Piligkos, S. K. Singh, D. Larsen, M. Schau-Magnussen, G. Rajaraman, M. Evangelisti, J. Bendix, *Angew. Chem. Int. Ed.* **2014**, *53*, 2394 – 2397; *Angew. Chem.* **2014**, *126*, 2426 – 2429; d) K. R. Vignesh, S. K. Langley, K. S. Murray, G. Rajaraman, *Chem. Eur. J.* **2015**, *21*, 2881 – 2892; e) T. Pugh, N. F. Chilton, R. A. Layfield, *Angew. Chem. Int. Ed.* **2016**, *55*, 11082 – 11085.

[7] L. Sorace, C. Benelli, D. Gatteschi, *Chem. Soc. Rev.* **2011**, *40*, 3092 – 3104.

[8] Y.-C. Chen, J.-L. Liu, L. Ungur, Q.-W. Li, L.-F. Wang, Z.-P. Ni, L. F. Chibotaru, X.-M. Chen, M.-L. Tong, *J. Am. Chem. Soc.* **2016**, *138*, 2829 – 2837

[9] a) S. K. Singh, T. Gupta, G. Rajaraman, *Inorg. Chem.* **2014**, *53*, 10835 – 10845; b) T. Pugh, V. Vieru, L. F. Chibotaru, R. A. Layfield, *Chem. Sci.* **2016**, *7*, 2128 – 2137; c) T. Pugh, F. Tuna, L. Ungur, D. Collison, E. J. L. McInnes, L. F. Chibotaru, R. A. Layfield, *Nat. Commun.* **2015**, *6*, 7492.

[10] a) N. F. Chilton, D. Collison, E. J. L. McInnes, R. E. P. Winpenny, A. Soncini, *Nat. Commun.* **2013**, *4*; b) I. Oyarzabal, J. Ruiz, E. Ruiz, D. Aravena, J. M. Seco, E. Colacio, *Chem. Commun.* **2015**, *51*, 12353 – 12356; c) J. D. Rinehart, J. R. Long, *Chem. Sci.* **2011**, *2*, 2078 – 2085.

[11] R. E. P. Winpenny, in *Perspectives in Supramolecular Chemistry*, Wiley, New York, **1999**, pp. 193 – 223.

[12] F. Habib, G. Brunet, V. Vieru, I. Korobkov, L. F. Chibotaru, M. Murugesu, *J. Am. Chem. Soc.* **2013**, *135*, 13242 – 13245.

[13] a) S. K. Langley, N. F. Chilton, B. Moubaraki, K. S. Murray, *Chem. Commun.* **2013**, *49*, 6965 – 6967; b) S. K. Langley, N. F. Chilton, B. Moubaraki, K. S. Murray, *Inorg. Chem.* **2013**, *52*, 7183 – 7192; c) S. K. Langley, N. F. Chilton, B. Moubaraki, K. S. Murray, *Inorg. Chem. Front.* **2015**, *2*, 867 – 875; d) S. K. Langley, N. F. Chilton, L. Ungur, B. Moubaraki, L. F. Chibotaru, K. S. Murray, *Inorg. Chem.* **2012**, *51*, 11873 – 11881; e) S. K. Langley, C. Le, L. Ungur, B. Moubaraki, B. F. Abrahams, L. F. Chibotaru, K. S. Murray, *Inorg. Chem.* **2015**, *54*, 3631 – 3642; f) S. K. Langley, L. Ungur, N. F. Chilton, B. Moubaraki, L. F. Chibotaru, K. S. Murray, *Inorg. Chem.* **2014**, *53*, 4303 – 4315.

[14] a) J. P. Costes, S. Titos-Padilla, I. Oyarzabal, T. Gupta, C. Duhayon, G. Rajaraman, E. Colacio, *Chem. Eur. J.* **2015**, *21*, 15785 – 15796; b) J. P. Costes, S. Titos-Padilla, I. Oyarzabal, T. Gupta, C. Duhayon, G. Rajaraman, E. Colacio, *Inorg. Chem.* **2016**, *55*, 4428 – 4440; c) A. Upadhyay, S. K. Singh, C. Das, R. Mondol, S. K. Langley, K. S. Murray, G. Rajaraman, M. Shanmugam, *Chem. Commun.* **2014**, *50*, 8838 – 8841.

[15] S. K. Langley, C. M. Forsyth, B. Moubaraki, K. S. Murray, *Dalton Trans.* **2015**, *44*, 912 – 915.

[16] J. Rinck, G. Novitchi, W. Van den Heuvel, L. Ungur, Y. Lan, W. Wernsdorfer, C. E. Anson, L. F. Chibotaru, A. K. Powell, *Angew. Chem. Int. Ed.* **2010**, *49*, 7583 – 7587; *Angew. Chem.* **2010**, *122*, 7746 – 7750.

[17] N. P. Cowieson, D. Aragao, M. Clift, D. J. Ericsson, C. Gee, S. J. Harrop, N. Mudie, S. Panjikar, J. R. Price, A. Riboldi-Tunnicliffe, R. Williamson, T. Caradoc-Davies, *J. Synchrotron Radiat.* **2015**, *22*, 187 – 190.

[18] T. M. McPhillips, S. E. McPhillips, H.-J. Chiu, A. E. Cohen, A. M. Deacon, P. J. Ellis, E. Garman, A. Gonzalez, N. K. Sauter, R. P. Phizackerley, S. M. Soltis, P. Kuhn, *J. Synchrotron Radiat.* **2002**, *9*, 401 – 406.

[19] W. Kabsch, *J. Appl. Crystallogr.* **1993**, *26*, 795 – 800.

[20] G. Sheldrick, *Acta Crystallogr. Sect. A* **2008**, *64*, 112 – 122.

[21] G. M. Sheldrick, *SHELXL-97*, *Programs for X-ray Crystal Structure Refinement*; **1997**, University of Göttingen: Göttingen, Germany.

[22] L. J. Barbour, *J. Supramol. Chem.* **2001**, *1*, 189 – 191.

[23] F. Aquilante, T. B. Pedersen, V. Veryazov, R. Lindh, *WIREs Comput. Mol. Sci.* **2013**, *3*, 143 – 149.

[24] L. F. Chibotaru, L. Ungur, *J. Chem. Phys.* **2012**, *137*, 064112 – 064122.

[25] L. F. Chibotaru, L. Ungur, *Program POLY ANISO* **2006**, *##University of Leuven*.

[26] L. Noodleman, *J. Am. Chem. Soc.* **1981**, *74*, 5737 – 5743.

[27] a) S. Piligkos, G. Rajaraman, M. Soler, N. Kirchner, J. van Slageren, R. Bircher, S. Parsons, H.-U. Gudel, J. Kortus, W. Wernsdorfer, G. Christou, E. K. Brechin, *J. Am. Chem. Soc.* **2005**, *127*, 5572 – 5580; b) G. Rajaraman, J. Cano, E. K. Brechin, E. J. L. McInnes, *Chem. Commun.* **2004**, 1476 – 1477; c) E. Ruiz, J. Cano, S. Alvarez, P. Alemany, *J. Comput. Chem.* **1999**, *20*, 1391 – 1400; d) E. Ruiz, J. Cano, S. Alvarez, A. Caneschi, D. Gatteschi, *J. Am. Chem. Soc.* **2003**, *125*, 6791 – 6794; e) E. Ruiz, A. Rodríguez-Fortea, J. Cano, S. Alvarez, P. Alemany, *J. Comput. Chem.* **2003**, *24*, 982 – 989.

[28] a) N. Berg, T. Rajeshkumar, S. M. Taylor, E. K. Brechin, G. Rajaraman, L. F. Jones, *Chem. Eur. J.* **2012**, *18*, 5906 – 5918; b) S. Ghosh, S. K. Singh, S. Tewary, G. Rajaraman, *Dalton Trans.* **2013**, *42*, 16490 – 16493; c) G. Rajaraman, M. Murugesu, E. C. Sanudo, M. Soler, W. Wernsdorfer, M. Helliwell, C. Muryn, J. Raftery, S. J. Teat, G. Christou, E. K. Brechin, *J. Am. Chem. Soc.* **2004**, *126*, 15445 – 15457.

[29] a) T. Rajeshkumar, G. Rajaraman, *Chem. Commun.* **2012**, *48*, 7856 – 7858; b) S. K. Singh, T. Rajeshkumar, V. Chandrasekhar, G. Rajaraman, *Polyhedron* **2013**, *66*, 81 – 86.

[30] a) M. L. Baker, G. A. Timco, S. Piligkos, J. S. Mathieson, H. Mutka, F. Tuna, P. Kozlowski, M. Antkowiak, T. Guidi, T. Gupta, H. Rath, R. J. Woolfson, G. Kamieniarz, R. G. Pritchard, H. Weihe, L. Cronin, G. Rajaraman, D. Collison, E. J. L. McInnes, R. E. P. Winpenny, *Proc. Natl. Acad. Sci. USA* **2012**, *109*, 19113 – 19118; b) P. Christian, G. Rajaraman, A. Harrison, M. Helliwell, J. J. W. McDouall, J. Raftery, R. E. P. Winpenny, *Dalton Trans.* **2004**, 2550 – 2555; c) P. Christian, G. Rajaraman, A. Harrison, J. J. W. McDouall, J. T. Raftery, R. E. P. Winpenny, *Dalton Trans.* **2004**, 1511 – 1512; d) G. Rajaraman, E. Ruiz, J. Cano, S. Alvarez, *Chem. Phys. Lett.* **2005**, *415*, 6 – 9.

[31] W. Liu, H. H. Thorp, *Inorg. Chem.* **1993**, *32*, 4102 – 4105.

[32] C. Benelli, D. Gatteschi, *Chem. Rev.* **2002**, *102*, 2369 – 2388.

[33] B. N. Figgis, *Introduction to Ligand Fields*, Wiley, New York, **1966**.

[34] a) J. Cirera, E. Ruiz, S. Alvarez, *Chem. Eur. J.* **2006**, *12*, 3162 – 3167; b) M. Pinsky, D. Avnir, *Inorg. Chem.* **1998**, *37*, 5575 – 5582.

[35] H. L. C. Feltham, Y. Lan, F. Klöwer, L. Ungur, L. F. Chibotaru, A. K. Powell, S. Brooker, *Chem. Eur. J.* **2011**, *17*, 4362 – 4365.

[36] a) K. R. Vignesh, S. K. Langley, B. Moubaraki, K. S. Murray, G. Rajaraman, *Chem. Eur. J.* **2015**, *21*, 16364 – 16369; b) C. Das, S. Vaidya, T. Gupta, J. M. Frost, M. Righi, E. K. Brechin, M. Affronte, G. Rajaraman, M. Shanmugam, *Chem. Eur. J.* **2015**, *21*, 15639 – 15650.

[37] S. K. Langley, D. P. Wielechowski, V. Vieru, N. F. Chilton, B. Moubaraki, B. F. Abrahams, L. F. Chibotaru, K. S. Murray, *Angew. Chem. Int. Ed.* **2013**, *52*, 12014 – 12019; *Angew. Chem.* **2013**, *125*, 12236 – 12241.
[38] a) S. K. Singh, M. F. Beg, G. Rajaraman, *Chem. Eur. J.* **2016**, *22*, 672 – 680; b) S. K. Singh, N. K. Tibrewal, G. Rajaraman, *Dalton Trans.* **2011**, *40*, 10897 – 10906.
[39] S. K. Singh, K. S. Pedersen, M. Sigrist, C. A. Thuesen, M. Schau-Magnussen, H. Mutka, S. Piligkos, H. Weihe, G. Rajaraman, J. Bendix, *Chem. Commun.* **2013**, *49*, 5583 – 5585.
[40] a) T. Rajeshkumar, H. V. Annadata, M. Evangelisti, S. K. Langley, N. F. Chilton, K. S. Murray, G. Rajaraman, *Inorg. Chem.* **2015**, *54*, 1661 – 1670; b) G. Rajaraman, F. Totti, A. Bencini, A. Caneschi, R. Sessoli, D. Gatteschi, *Dalton Trans.* **2009**, 3153 – 3161.
[41] S. K. Singh, G. Rajaraman, *Dalton Trans.* **2013**, *42*, 3623 – 3630.
[42] T. Gupta, G. Rajaraman, *Chem. Commun.* **2016**, *52*, 8972 – 9008.
[43] Note that the quoted values are U_{cal} values, except for complex **4** for which the U_{eff} value is given.

Manuscript received: October 14, 2016
Accepted Article published: November 18, 2016
Final Article published: January 4, 2017